

# Design of an arrangement of cubic magnets for a quasi-axisymmetric stellarator experiment

K. C. Hammond,<sup>1,\*</sup> C. Zhu,<sup>1,2</sup> K. Corrigan,<sup>1</sup> D. A. Gates,<sup>1</sup>  
R. Lown,<sup>3</sup> R. Mercurio,<sup>3</sup> T. M. Qian,<sup>1</sup> and M. C. Zarnstorff<sup>1</sup>

<sup>1</sup>*Princeton Plasma Physics Laboratory, Princeton, NJ 08543, USA*

<sup>2</sup>*Present affiliation: Department of Plasma Physics and Fusion Engineering,  
School of Nuclear Science and Technology, University of Science and Technology of China, Hefei 230026, China*

<sup>3</sup>*SABR Enterprises, LLC, North Andover, MA 01845, USA*

The usage of permanent magnets to shape the confining magnetic field of a stellarator has the potential to reduce or eliminate the need for non-planar coils. As a proof-of-concept for this idea, we have developed a procedure for designing an array of cubic permanent magnets that works in tandem with a set of toroidal-field coils to confine a stellarator plasma. All of the magnets in the design are constrained to have identical geometry and one of three polarization types in order to simplify fabrication while still producing sufficient field accuracy. We present some of the key steps leading to the design, including the geometric arrangement of the magnets around the device, the procedure for optimizing the polarizations according to the three allowable magnet types, and the choice of magnet types to be used. We apply these methods to design an array of rare-Earth permanent magnets that can be paired with a set of planar toroidal-field coils to confine a quasi-axisymmetric plasma with a toroidal magnetic field strength of about 0.5 T on axis.

## I. INTRODUCTION

The stellarator is a magnetic fusion reactor concept that seeks to confine a burning plasma with a precisely-shaped, non-axisymmetric magnetic field. The most advanced stellarator designs to date have typically relied on complex, non-planar coils to generate this field. Since non-planar coils have been a major driver of cost and construction time for stellarator experiments [1–3], methods for achieving desired magnetic fields with simpler coil geometry have been a major area of research [4–13]. Recently, permanent magnets were proposed as an approach to coil simplification [14]. In principle, permanent magnets can contribute to the three-dimensional shaping of the magnetic field, thereby easing the shaping requirements for any non-planar coils or even eliminating the need for non-planar coils altogether.

Many strategies for designing suitable magnet arrays have been developed. Some approaches entailed calculating a spatial distribution of magnetization throughout a three-dimensional layer surrounding a winding surface that encloses the target plasma [15–17]. These procedures typically employ a Fourier representation of the magnetization distribution and as such share much in common with methods for designing modular coils for stellarators [8, 18]. Other approaches optimize the dipole moments of discrete magnets in arbitrary locations [19–22].

In all of these cases, the distribution of magnetization  $\mathbf{M}$  through the magnet arrangement is determined through an optimization procedure. The spatial distribution of  $\mathbf{M}$  is defined parametrically, e.g. through Fourier harmonics or through the moments of individual dipoles in the arrangement. The optimization procedure adjusts these parameters to minimize the normal component of the total magnetic field on the boundary of the targeted plasma equilibrium, including contributions from the permanent magnets, toroidal-field (TF) coils, any additional coils, and plasma currents.

To reduce the complexity and cost of magnet fabrication, it is preferable to minimize the number of unique magnet types required for an arrangement, both in terms of geometry and magnetization. Formulating and imposing such constraints on the optimization procedure is a nontrivial endeavor, and one that admits multiple possible strategies. One approach has been to constrain the polarization of each magnet

\* khammond@pppl.gov

to be locally normal to a winding surface that encloses the plasma and conforms to the plasma's boundary geometry [15, 17, 20]. In such a scheme, the magnets could be cut from thin slabs of uniformly-polarized magnetic material and oriented to be locally normal to the winding surface. The drawback of such a constraint is that the solution tends to make less efficient use of the magnets than solutions that find the optimal polarization direction at each location. Hence, while this approach works well for target plasmas with relatively low three-dimensional field shaping requirements [15, 20, 22], a greater degree of freedom in the polarization direction may be necessary if stronger shaping fields are required or if engineering constraints limit the amount of magnet material that can be placed near the plasma boundary [23].

For magnet array designs in which the polarization direction is optimized, the magnet shapes and their spatial layout can be more easily decoupled from a toroidal winding surface. This enables the use of simpler and fewer different magnet shapes and mounting structures. However, to limit the total number of unique magnet types required, the polarization cannot be allowed to vary continuously for each magnet and must instead be chosen from a discrete set of allowable polarizations. If each magnet is constrained to have a cubic shape with a polarization along an axis of symmetry perpendicular to two of its faces, this would enable solutions in which only one unique magnet type is required, as recently demonstrated by Lu et al. [21]. An alternative method for optimizing magnet arrays with discrete polarizations will be presented in this paper.

In this work, we utilize these advances in discrete magnet optimization to design a magnet array for a mid-scale quasi-axisymmetric stellarator in which the magnetic field is created with permanent magnets and planar TF coils. The array consists of three unique types of magnets, each with identical cubic geometry and distinguished only by its polarization orientation. The magnets are designed to confine a variant of the "C09R00" equilibrium, originally designed for the NCSX experiment [24, 25], with the magnetic field on axis scaled down to about 0.5 T. Correspondingly, the magnet array will be constrained to fit around the NCSX vacuum vessel. In addition, it will be assumed that the NCSX TF coils are to provide the toroidal component of the magnetic field; no other coils will be incorporated into the design. The target plasma has a major radius of 1.44 m, a minor radius of 0.32 m, and a volume-averaged beta of 4.1%.

## II. OUTLINE OF THE DESIGN AND OPTIMIZATION PROCEDURE

The procedure developed in this work for specifying a magnet arrangement can be summarized as follows:

1. Generate an arrangement of cubic magnets
2. Perform a continuous optimization of the dipole moments of each magnet in two steps:
  - (a) Minimize an objective function for magnetic field inaccuracy
  - (b) Minimize a weighted sum of objective functions for field inaccuracy and intermediate dipole moment magnitudes
3. Rotate each optimized moment vector to the nearest allowable discrete vector

The remainder of this paper will describe each of these steps in more detail and present the results of the application of this procedure to the design of a magnet array for the target plasma. Sec. III will describe the geometric arrangement of the magnets around the plasma vessel. Sec. IV will describe the procedures used to perform continuous optimizations of the dipole moments of each magnet. Sec. V will describe the polarization types that were considered for the discrete solution and explain the down-selection to the three types used for the magnet array design.

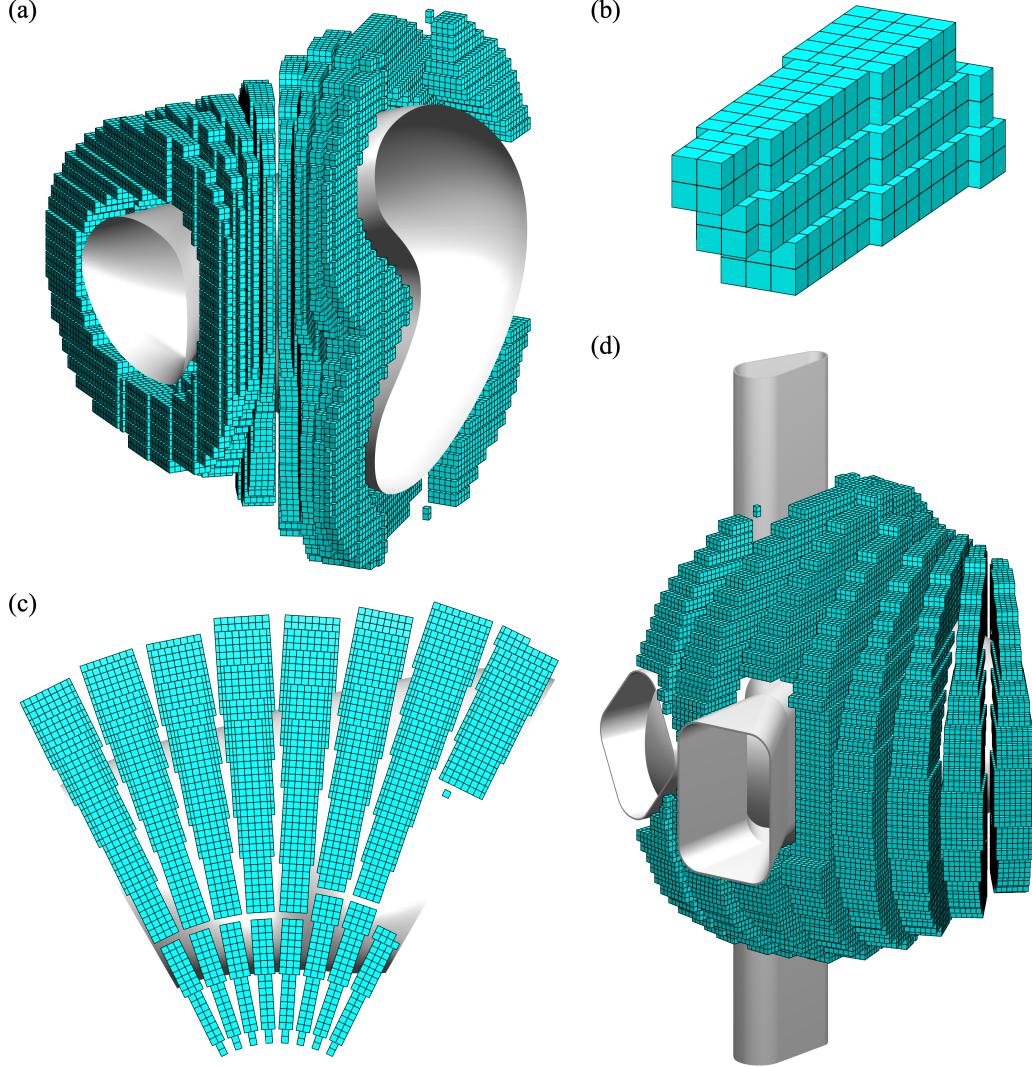


FIG. 1. Arrangement of cubic magnets designed to conform to one half-period of the NCSX vacuum vessel, which extends  $60^\circ$  toroidally. (a) view from the inboard side; (b) close-up view of three vertically-stacked “drawers” of magnets from the inboard side; (c) view from the top; (d) view from the outboard side, including ports that the magnets were designed to avoid

### III. MAGNET LAYOUT AND MOUNTING CONCEPT

The scheme for the spatial layout of the magnets seeks to pack magnets as tightly as possible around the plasma-conforming vacuum vessel, as magnets positioned close to the plasma provide the required three-dimensional magnetic field shaping more efficiently. At the same time, the layout must be compatible with reasonably simple concepts for fabrication, assembly, and mounting. As such, the layout scheme was developed in close coordination with the design of the mounting structures.

An example arrangement of cubic magnets is shown in Fig. 1. The magnets are divided into a set of discrete wedges, each of which subtends a particular toroidal angle (Fig. 1c). The magnets in each wedge are partitioned into an inboard and outboard subset, with the inboard/outboard boundaries determined separately on the top and bottom according to proximity to the highest and lowest points of the cross-section

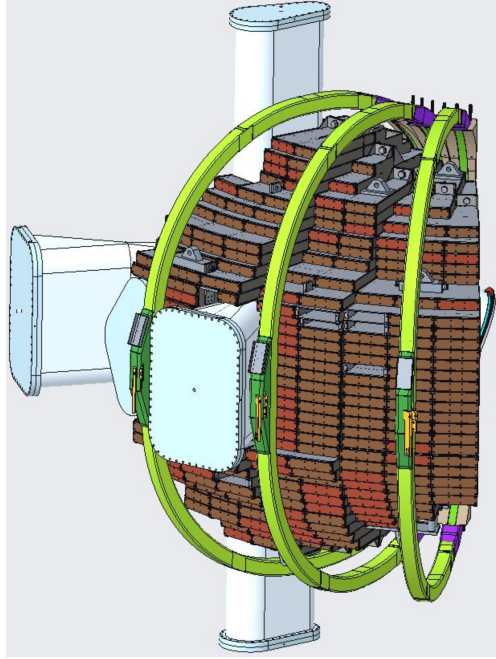


FIG. 2. Rendering of the permanent magnet mounting structure positioned around the plasma vessel. The magnets are fully enclosed within this structure. The vantage point for this image is similar to that of Fig. 1d. The structures fit within the bore of the toroidal-field coils, which are shown in yellow.

of the plasma vessel. Within each partition, the magnets are subdivided into “drawers,” each of which is two layers high (Fig. 1b). Magnets within each drawer are held together with glue. The drawers are inserted in gridded structures on both the inboard and outboard sides of the vessel.

The magnets were restricted to be cubic in shape in order to take advantage of the cube’s many degrees of rotational symmetry. This allows for many different dipole moment directions to be realized at each location in the magnet arrangement using various orientations of a small number of unique magnet polarization types. The edge length of the cube was set at 3 cm, and was limited by the fabrication procedure. Specifically, the magnets are foreseen to be cut from a 5 cm slab of material with a polarization orientation perpendicular to the slab plane. Hence, to obtain a cube with a polarization that is not perpendicular to a face, it must be cut at an oblique angle from the slab. Our design utilizes three different polarization types, two of which are not perpendicular to a face. 3 cm is the largest possible edge length for cubes of each of these orientations to be cut from the slab. Our choice of these polarization types will be discussed in more detail in Sec. V.

The spacing between adjacent magnets was set to accommodate the methods for mounting and assembly. Magnets within the same drawer are separated by a distance of 0.04 cm to leave space for glue as well as a thin coating layer on each magnet. To leave room for the gridded mechanical support structure, depicted in Fig. 2, adjacent drawers are separated by 0.97 cm in the vertical dimension and a minimum of 1.59 cm in the toroidal dimension. Further details on the design of the support structure, as well as the finite-element calculations performed to qualify the structure for withstanding gravitational and internal magnetic forces, will be given in a separate paper [26].

Design of the magnet layout was facilitated by the MAGPIE code [23], which was upgraded to accommodate the present concept with cubic magnets. The code can position magnets around any smooth toroidal surface, so the layout scheme can be easily generalized to any stellarator with a plasma-conforming containment vessel. Parameters such as the thickness of the magnet layer, the width of the gap spacing between adjacent magnets, and the number of toroidal wedges may be chosen by the user to best suit the physics

requirements and engineering constraints. Magnets may also be excluded from regions that would collide with other objects, such as toroidal-field coils or access ports.

#### IV. CONTINUOUS MAGNET OPTIMIZATION

Once the positions of the magnets in the arrangement are specified, their dipole moments are optimized to create the magnetic field shaping required to confine a plasma in a given target equilibrium. For simplicity of fabrication, the number of unique magnet types is restricted: all magnets are cubes with identical dimensions and one of a small number of polarization orientations. Hence, the space of possible solutions is discrete and has a large number of degrees of freedom that scales with the number of magnets (of which there are typically tens of thousands). Finding an optimal solution within this large, discrete space is a challenging computational task. Our approach to this problem divides the optimization procedure into a few steps. The first steps are continuous optimizations that take advantage of gradient-based algorithms. The continuous solutions are then projected into the discrete space of allowable magnet types. This section describes the first steps of the process, which employ continuous optimization.

The continuous optimizations were carried out by the FAMUS code [19]. FAMUS models each magnet as an ideal dipole with moment  $\mathbf{m} = \rho MV \hat{\mathbf{v}}(\phi, \theta)$ , where  $\rho$  is a scaling constant,  $M$  is the magnetization,  $V$  is the volume of the permanent magnet represented by the dipole, and  $\hat{\mathbf{v}}(\phi, \theta)$  is a unit vector whose orientation is specified by an azimuthal angle  $\phi$  and polar angle  $\theta$ . The magnetization  $M$  can be related to the remanent field  $B_r$  of the permanent magnet through  $B_r = \mu M$ , where  $\mu$  is the permeability. To simplify the optimization, any deviation of the magnets' permeability from that of free space is neglected; hence,  $\mu = \mu_0$ . The calculations in this paper assume a remanent field  $B_r = 1.38$  T, consistent with typical rare-Earth permanent magnets. Additional contributions to the magnetic field from the toroidal field coils and from currents within the target plasma were held fixed during the optimizations.

The continuous optimizations proceeded in two steps, distinguished primarily by the objective function that the optimizer sought to minimize. In the first step, the parameters  $\rho$ ,  $\theta$ , and  $\phi$  for each dipole were adjusted to minimize the magnetic field error, quantified by the surface integral

$$\chi_B^2 = \iint_{\mathcal{S}} (\mathbf{B} \cdot \hat{\mathbf{n}})^2 dA, \quad (1)$$

where  $\mathcal{S}$  is boundary of the target plasma,  $\hat{\mathbf{n}}$  is the unit vector normal to  $\mathcal{S}$ , and  $\mathbf{B}$  is the total magnetic field evaluated on  $\mathcal{S}$ , including contributions from the toroidal field coils, plasma current, and the permanent magnets. Note that targeted magnetic field is perfectly achieved if  $\chi_B^2 = 0$ . For each magnet, the scaling parameter  $\rho$  was constrained to remain between  $-1$  and  $1$ , inclusive, such that the magnitude  $|\mathbf{m}|$  of each dipole moment never exceeded  $MV$ . The parameter  $\rho$  was initialized to zero for each magnet, whereas the angles  $\theta$  and  $\phi$  were initialized so that each dipole was approximately aligned with the normal vector of a nearby point on the plasma vessel.

At the end of this first step, the solution should attain a certain minimum level of field accuracy to be considered viable. For the studies in this paper, we have chosen the following criterion for sufficient field accuracy:

$$b_n = \frac{1}{B_0 A} \iint_{\mathcal{S}} |\mathbf{B} \cdot \hat{\mathbf{n}}| dA \leq 0.005 \quad (2)$$

Here,  $b_n$  is the normalized surface-averaged normal component of the total magnetic field on the target plasma boundary,  $A$  is the surface area of the plasma boundary, and  $B_0$  is the approximate value of the magnetic field on the target plasma's magnetic axis, which is 0.5 T for our target plasma equilibrium. The choice of  $b_n \leq 0.005$  as the criterion was informed by free-boundary equilibrium modeling of magnet

solutions with a range of  $b_n$  values. Should the optimized magnet solution fail to meet the criterion at this stage, the geometric arrangement would need to be modified, typically by increasing the thickness of the magnet layer and/or increasing the concentration of magnets close to the plasma.

If the first step succeeds in meeting the criterion, a second step is performed to find a refined solution in which the optimized values of  $\rho$  have an absolute value of either 1 or 0. Attaining such a binary distribution of  $|\rho|$  for the set of dipoles is an important step on the way to a discrete solution. If every dipole has either zero strength or full strength  $|\mathbf{m}| = MV$ , the solution can be realized by placing magnets with a uniform volume  $V$  at the locations of dipoles with  $|\rho|=1$  and by simply leaving empty the locations of dipoles with  $\rho = 0$ . If, on the other hand, the solution had many dipoles with intermediate  $|\rho|$  values, it would be necessary to use magnets with a wide range of volumes  $V$ , which is incompatible with the requirement of using magnets with identical dimensions.

To this end, the dipole moment parameters are put through a second continuous optimization that minimizes a linear combination of two objective functions:  $\chi_B^2 + \lambda \chi_\rho^2$ , where

$$\chi_\rho^2 = \sum_i^N (|\rho_i|(1 - |\rho_i|))^2, \quad (3)$$

$N$  is the number magnets whose dipole moments are to be optimized,  $i$  is the index number for each magnet, and  $\rho_i$  is the scaling constant for the moment magnitude of the  $i^{th}$  magnet. As can be seen in Eq. 3, the objective function  $\chi_\rho^2$  favors magnets with  $\rho = 0$  or  $|\rho| = 1$  and penalizes magnets with intermediate values of  $|\rho|$ . The weighting factor  $\lambda$ , which is held fixed during the optimization, is chosen so that the solution retains good field accuracy while eliminating the presence of magnets with intermediate moment magnitudes. In practice, the optimization must be repeated with different values of  $\lambda$  until a suitable trade-off is found.

Traces of the objective functions from an optimization of the dipole moments of the magnets in the arrangement from Fig. 1 are shown in Fig. 3. The dipole moments in this case were optimized for the target plasma, and the objective function  $\chi_B^2$  was computed accordingly (Eq. 1). In the first step, in which the optimizer seeks to exclusively minimize field error,  $\chi_B^2$  decreased by almost four orders of magnitude (Fig. 3a). In the second step, in which a weighted sum of  $\chi_B^2$  and  $\chi_\rho^2$  is minimized,  $\chi_\rho^2$  undergoes a reduction of nearly four orders of magnitude while avoiding an increase of  $\chi_B^2$ , which in fact improves slightly (Fig. 3b).

The effects of the two optimization steps on the distribution of dipole moment magnitudes can be seen in Fig. 4. After the first step (Fig. 4a), just under half of the 58,258 dipoles in the arrangement have attained the maximum moment magnitude allowed by the optimization procedure, corresponding to  $|\rho| = 1$ . The rest of the distribution is broadly spread among intermediate values of  $|\rho|$ . Then, after the second step (Fig. 4b), the intermediate values of  $|\rho|$  have largely been removed from the distribution, with all dipole moments having a magnitude of nearly zero or the maximum value.

## V. MAPPING DIPOLE MOMENTS TO A DISCRETE SUBSET

Following the continuous optimization steps in Sec. IV, the dipole moments in the magnet array exhibit a nearly binary distribution of magnitude, but the directions of each vector are unrestricted. To limit the number of polarization types required in the array, the directions must be adjusted to the nearest direction permitted by a discrete set of polarization types. Since this adjustment entails moving the vectors away from their optimal orientations, it will reduce the magnetic field accuracy of the array. Hence, using a larger number of polarization types would require smaller adjustments to the optimized moment directions and therefore enable greater field accuracy. However, the need for field accuracy must be balanced against the added complexity of fabricating magnets with many different polarization types.

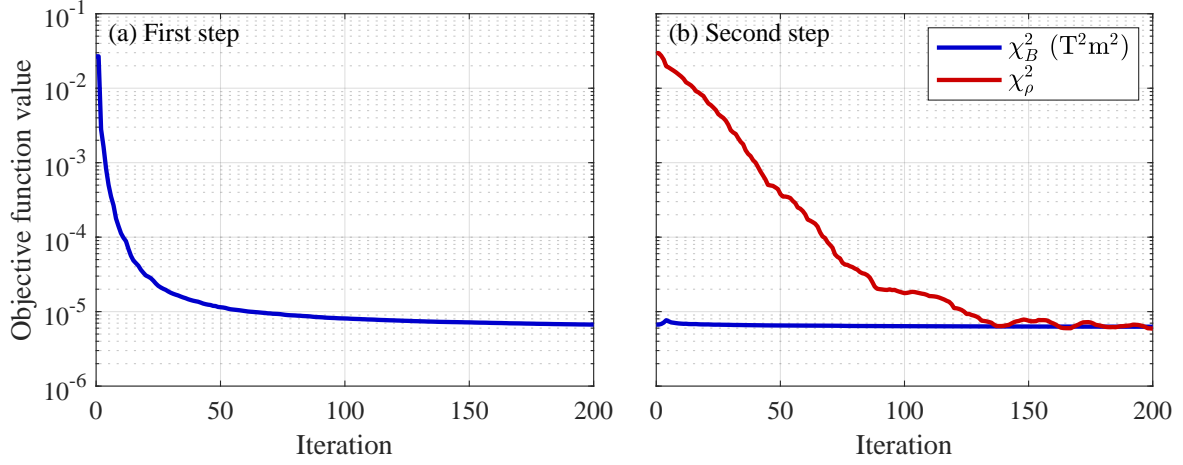


FIG. 3. Values of the objective functions  $\chi_B^2$  and  $\chi_\rho^2$  during a two-step continuous optimization of the dipole moments of the magnet arrangement shown in Fig. 1 for the target plasma. (a) first step, in which only  $\chi_B^2$  was minimized; (b) second step, which continued from the end point of the first step while minimizing a linear combination of  $\chi_B^2$  and  $\chi_\rho^2$ .

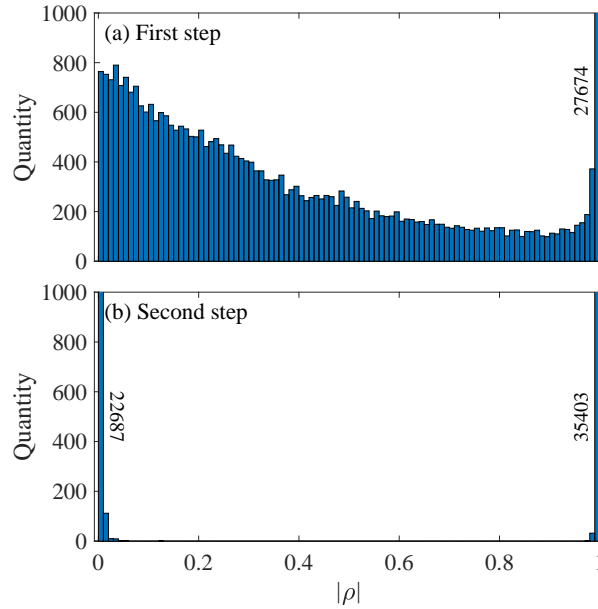


FIG. 4. Histograms of normalized dipole moment magnitude  $|\rho|$  for a set of magnets following (a) the first step and (b) the second step of a continuous optimization of the magnets in the arrangement shown in Fig. 1 for the target plasma. Bin quantities that exceed the y-axis limit are written alongside the respective bin.

This section describes the assessment and selection of polarization types for the discrete solution. Sec. V A describes the six types considered in this work. Sec. V B describes the different subsets of those six types that were evaluated for discrete solutions. Sec. V C presents a comparison of discrete solutions for the target plasma employing the different subsets of types, with a focus on the subset of three types (which will be identified as “Subset 5” in Sec. V B) that we ultimately chose for the magnet array design.

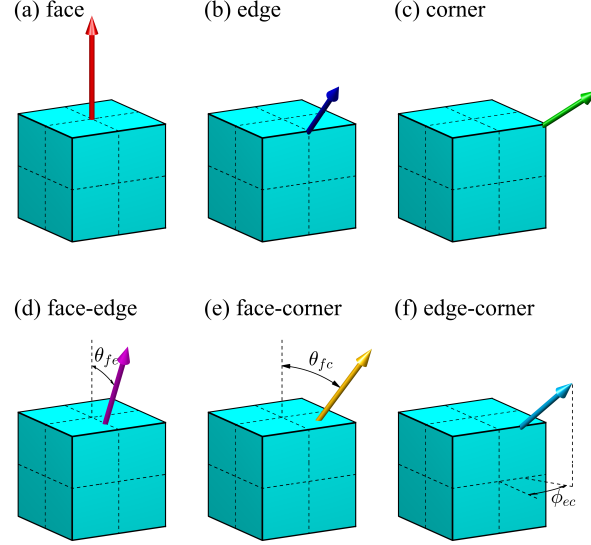


FIG. 5. Polarization orientations relative to the cubic geometry of the magnet types considered for this study.

### A. Magnet polarization types

The six polarization types considered in this work are shown in Fig. 5. The *face* type (Fig. 5a) exhibits a magnetization represented by a unit vector  $\hat{\mathbf{v}}_f$  perpendicular to the planes of two opposite faces. This type admits six distinct dipole moment vectors from the possible rotations of the cube that preserve the cube's geometric orientation. The *edge* type (Fig. 5b) exhibits a magnetization vector  $\hat{\mathbf{v}}_e$  such that a line traced from the cube's centroid in this direction would intersect the midpoint of an edge. This type admits twelve different polarizations. The *corner* type (Fig. 5c) has a polarization vector  $\hat{\mathbf{v}}_c$  such that a line traced from the centroid in this direction would intersect one of the cube's corners. It admits eight different polarizations.

We also considered three “hybrid” polarization types that lie in planes defined by pairs of the basic types introduced above. The *face-edge* type (Fig. 5d) has a polarization vector  $\hat{\mathbf{v}}_{fe}$  that is coplanar with a face-type unit vector  $\hat{\mathbf{v}}_f$  and an edge-type unit vector  $\hat{\mathbf{v}}_e$ , and is specified by the angle

$$\theta_{fe} = \arccos(\hat{\mathbf{v}}_{fe} \cdot \hat{\mathbf{v}}_f) \quad (4)$$

to the nearest face-type vector. Assuming  $0 < \theta_{fe} < 45^\circ$ , there are twenty-four distinct polarization vectors obtainable through different rotations of the cube. The *face-corner* type (Fig. 5e) has a polarization vector  $\hat{\mathbf{v}}_{fc}$  that is coplanar with a face-type unit vector  $\hat{\mathbf{v}}_f$  and a corner-type unit vector  $\hat{\mathbf{v}}_c$ , and is specified by the angle

$$\theta_{fc} = \arccos(\hat{\mathbf{v}}_{fc} \cdot \hat{\mathbf{v}}_f) \quad (5)$$

to the nearest face-type vector. This admits twenty-four distinct vectors through rotations if  $0 < \theta_{fc} < \arccos(1/\sqrt{3}) \approx 54.7^\circ$ . Finally, the *edge-corner* type (Fig. 5f) lies in a plane parallel to an edge-type vector  $\hat{\mathbf{v}}_e$  and a corner-type vector  $\hat{\mathbf{v}}_c$ , and is specified by the azimuthal displacement angle  $\phi_{ec}$  that may be expressed as



Subset	F	E	C	FE	FC	EC	$\theta_{fe}$	$\theta_{fc}$	$\phi_{ec}$	Num. of polarizations	Max. $\theta_{\text{offs}}$ (deg.)	$\ \theta_{\text{offs}}\ _2$ (deg.)
1	✓									6	54.7	34.0
2	✓	✓								18	35.2	19.9
3	✓	✓	✓							26	27.5	16.6
4	✓	✓		✓			22.5			42	35.2	16.2
5	✓			✓	✓		30.3	38.1		54	19.4	11.3
6		✓		✓	✓		18.4	38.6		60	18.4	10.6
7	✓	✓		✓	✓		22.5	38.6		66	16.9	10.2
8	✓	✓	✓	✓	✓	✓	22.5	27.0	22.5	98	14.1	8.50

TABLE I. Properties of the subsets of polarization types considered in this work. Check marks indicate the presence of a given type in each subset. The types are abbreviated as follows: F=face, E=edge, C=corner, FE=face-edge, FC=face-corner, and EC=edge-corner. Angular parameters for the hybrid types ( $\theta_{fe}$ ,  $\theta_{fc}$ ,  $\phi_{ec}$ ), as defined in Sec. V A and Fig. 5, are given if their respective types are included in the subset.

$$\phi_{ec} = \arcsin \left( \frac{\mathbf{p}_e \times \mathbf{p}_{ec}}{|\mathbf{p}_e| |\mathbf{p}_{ec}|} \right), \quad (6)$$

where  $\mathbf{p}_e$  and  $\mathbf{p}_{ec}$  are the projections of  $\hat{\mathbf{v}}_e$  and  $\hat{\mathbf{v}}_{ec}$  onto the plane perpendicular to the adjacent face-type vector  $\hat{\mathbf{v}}_f$  for which  $\hat{\mathbf{v}}_f \cdot (\hat{\mathbf{v}}_e \times \hat{\mathbf{v}}_{ec})$  is positive. Assuming  $0 < \phi_{ec} < 45^\circ$ , there are twenty-four attainable polarization vectors  $\hat{\mathbf{v}}_{ec}$  from different rotations of the cube, as with  $\hat{\mathbf{v}}_{fe}$  and  $\hat{\mathbf{v}}_{fc}$ .

## B. Subsets of polarization types

A major choice that must be made in this design process is which, and how many, of the magnet polarization types to admit in the discrete solution. In general, employing more types implies more possible polarization vectors for each position in the magnet array, admitting solutions that can attain higher field accuracy and utilize the magnet material more efficiently. On the other hand, a larger number of polarization types leads to greater design complexity. Furthermore, certain polarization types are substantially more expensive to fabricate than others, depending primarily on how many of the cube's faces the polarization aligns with. For example, the face-type polarization is the simplest and cheapest to fabricate, whereas the edge-corner type would be the most complex and expensive. Hence, the choice of types to utilize needs to balance the physics requirement for field accuracy against the costs of fabrication.

To inform this choice, eight different subsets of the polarization types were evaluated for their attainable field accuracy. The subsets are summarized in Table I. The subsets ranged from the simplest possible, containing only the face-type polarization (Set 1) to containing all six types (Set 8).

The number of polarizations in Table I indicates the number of unique dipole moment vectors that can be created at a given position in the magnet array, given a choice of magnets of the types of polarizations within the subset and considering all possible orientations of the cube that maintain its geometric footprint. For example, when using Subset 1, which only contains magnets with the face-type polarization, six different dipole moment vectors can be created at a given position in the array. When using Subset 2, by contrast, either a face-type or an edge-type polarized magnet may be placed at each position. This yields a total of eighteen possible diople moment vectors (six for the face type and twelve for the edge type).

The discretization procedure described here entails rotating continuously-optimized dipole moment vectors to the nearest possible vectors from a discrete subset. Thus, the dipole moments output from the discretization procedure will have an angular offset,  $\theta_{\text{offs}}$ , from the original direction. Correspondingly, a given subset of polarization types can be characterized by its distribution of  $\theta_{\text{offs}}(\phi, \theta)$  over the unit sphere,

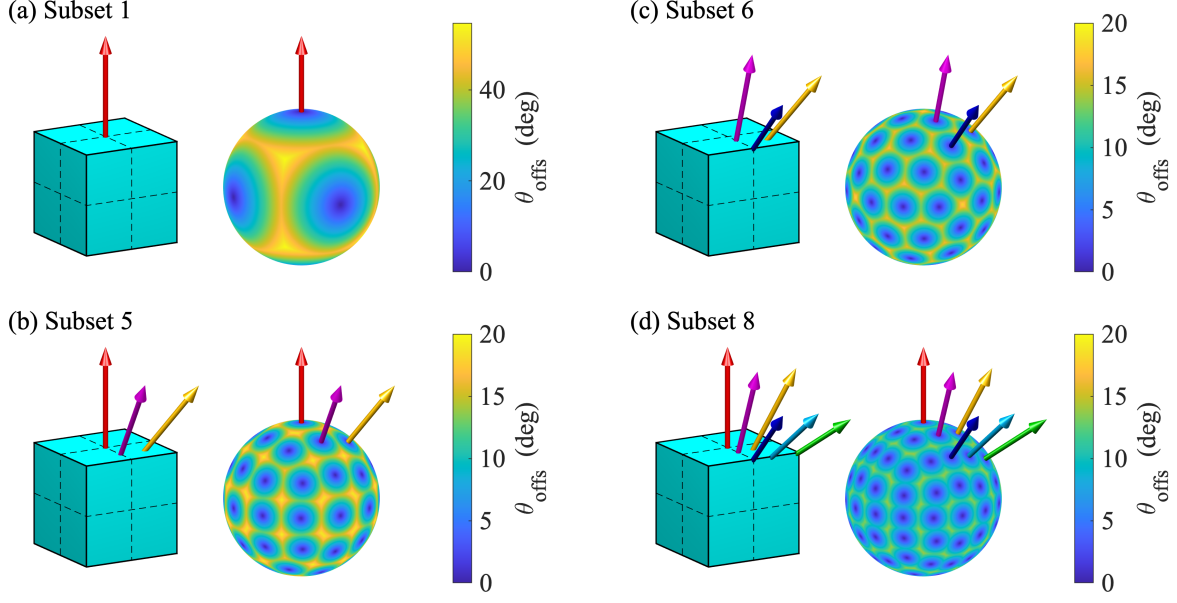


FIG. 6. Example polarization vectors relative to a cubic magnet (left side of each subfigure) and distribution of  $\theta_{\text{offs}}$  over the unit sphere (right side) for a selection of the polarization type subsets specified in Table I. Note that the color scale for Subset 1 (a) is different from that of the others (b)-(d).

parametrized by the azimuthal angle  $\phi$  and polar angle  $\theta$ . Formally,  $\theta_{\text{offs}}$  is the distribution of the angular separation from the nearest allowable dipole moment from the set of polarization types:

$$\theta_{\text{offs}}(\phi, \theta) = \min_{\hat{\mathbf{v}}_s \in S} [\arccos(\hat{\mathbf{v}}(\phi, \theta) \cdot \hat{\mathbf{v}}_s)] \quad (7)$$

Here,  $S$  contains all available polarization unit vectors  $\hat{\mathbf{v}}_s$  within a given subset of polarization types.  $\hat{\mathbf{v}}(\phi, \theta)$  is a unit vector representing the direction of an arbitrary, continuously-optimized dipole moment.

Distributions of  $\theta_{\text{offs}}$  from a few subsets of polarization types are shown in Fig. 6. The distributions are each plotted on spherical domains. For visual reference, an example of each type of polarization vector in the set is also shown. In addition, the reference vectors are shown relative to the geometry of a cubic magnet to the left of each sphere. Each allowable polarization vector within a subset appears as a local minimum of  $0^\circ$  in the distribution of  $\theta_{\text{offs}}$ . Naturally, the greatest values of  $\theta_{\text{offs}}$  are seen for the subsets with the fewest allowable polarization vectors.

The distribution of  $\theta_{\text{offs}}$  can be used to define two figures of merit for each subset of polarization types. The first is simply the maximum value of  $\theta_{\text{offs}}$  found on the unit sphere for a given subset. The second is the root-mean-square of  $\theta_{\text{offs}}$  over the domain:

$$\|\theta_{\text{offs}}\|_2 = \sqrt{\frac{1}{4\pi} \int_0^\pi \int_0^{2\pi} \theta_{\text{offs}}^2 \sin \theta \, d\phi \, d\theta} \quad (8)$$

Both of these quantities are shown for each set in Table I. They were estimated numerically on a grid of  $\phi$  and  $\theta$  values; the former by simply finding the maximum value of  $\theta_{\text{offs}}$  on the grid, and the latter through numerical integration.

Note that these quantities are functions of the polarization type subsets alone and are independent of the properties of any magnet array or target plasma. Nevertheless, it is reasonable to expect that subsets

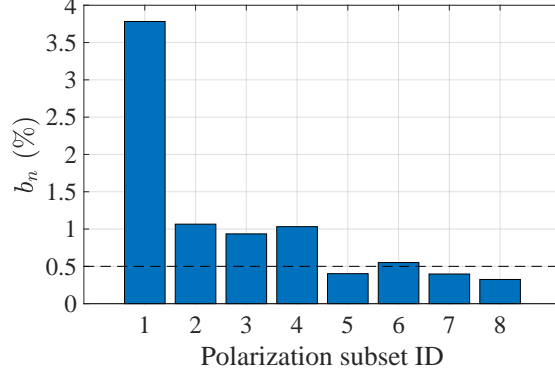


FIG. 7. Value of  $b_n$  (Eq. 2) on the boundary of the target plasma equilibrium after rotating the continuously-optimized dipole moments of the magnet array to each of the sets of polarization types specified in Table I. The horizontal dashed line indicates the criterion for field accuracy defined in Eq. 2.

with lower values of  $\|\theta_{\text{offs}}\|_2$  will generally introduce less error during the discretization procedure. Hence,  $\|\theta_{\text{offs}}\|_2$  helped to inform the design of some of the subsets. In particular,  $\theta_{\text{fe}}$  and  $\theta_{\text{fc}}$  for Subsets 5 and 6 were both chosen to minimize  $\|\theta_{\text{offs}}\|_2$ .

### C. Discretized solutions

The continuously-optimized dipole moments for the target plasma were discretized to polarizations from each of the eight subsets summarized in Table I. The magnetic field error of each of these discretized solutions, indicated by  $b_n$  (Eq. 2), is shown in Fig. 7. The predominant trend is that  $b_n$  tends to decrease as the number of available polarizations increases, and as the  $\|\theta_{\text{offs}}\|_2$  metric decreases. This is to be expected, as sets with more polarization options and lower offset angles tend to enable discrete solutions that are closer to the continuously-optimized solutions that they approximate. On the other hand, the dependence of  $b_n$  on  $\|\theta_{\text{offs}}\|_2$  is not perfectly monotonic: for example, Subset 6 exhibits a lower  $\|\theta_{\text{offs}}\|_2$  than Subset 5 (Table I), whereas the discretized solution utilizing Subset 5 attains a lower value of  $b_n$ . Note that overall, Subsets 5, 7, and 8 have satisfied the criterion for field accuracy defined in Eq. 2.

For a more detailed look at the suitability of the different solutions for confining the target plasma, we performed free-boundary magnetohydrodynamic (MHD) equilibrium calculations with the VMEC code [27, 28]. Each calculation assumed plasmas with the same prescribed toroidal current profile, pressure profile, and enclosed toroidal flux as the target plasma. The profiles of pressure and current are shown Fig. 9. The current profile is based on a neoclassical estimate of the bootstrap current for the target plasma [24]. The external magnetic fields for each plasma included contributions from the NCSX toroidal field coils and the permanent magnets, with each permanent magnet approximated as an ideal dipole. All modeled equilibria had volume-averaged  $\beta$  values of about 4.1%, similar to the target plasma. After the equilibrium properties were determined, the profile of effective ripple, a measure of neoclassical transport, was calculated using the NEO code [29].

Results of these calculations are shown in Fig. 8 for discrete solutions utilizing Subsets 1, 5, and 8, as well as the solution with continuous polarization angles used as input for the discretization. Key equilibrium properties are compared with those of the targeted plasma, including boundary geometry (Fig. 8a-b), rotational transform profile (Fig. 8c), and effective ripple profile (Fig. 8d). As expected, the worst agreement is found for the discrete solution using Subset 1, which contains only face-type magnets and therefore exhibits the greatest offsets from the continuously optimized dipole moments. By contrast, the discrete solutions with Subsets 5 and 8 yield plasma equilibria that are quite similar with that of the continuous

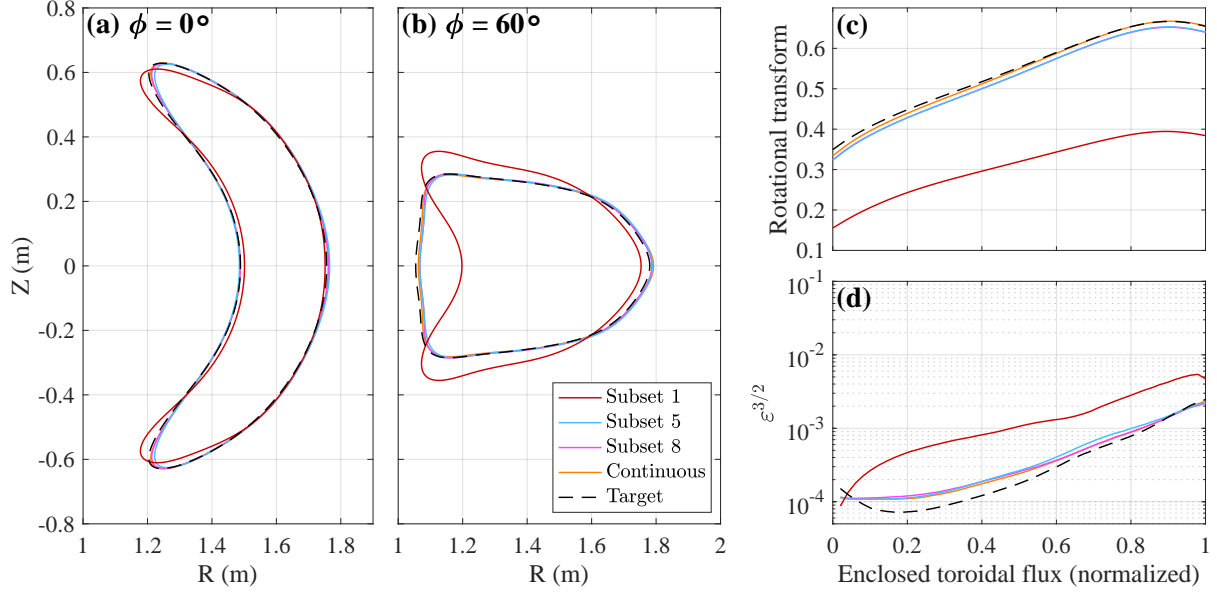


FIG. 8. Equilibrium properties of plasmas confined with the fields generated by selected magnet solutions as compared with the targeted plasma equilibrium. (a) Cross-sections of the plasma boundary at toroidal angle  $\phi = 0^\circ$ ; (b) Cross-sections of the plasma boundary at toroidal angle  $\phi = 60^\circ$ ; (c) Profiles of the rotational transform; and (d) Profiles of the effective ripple.

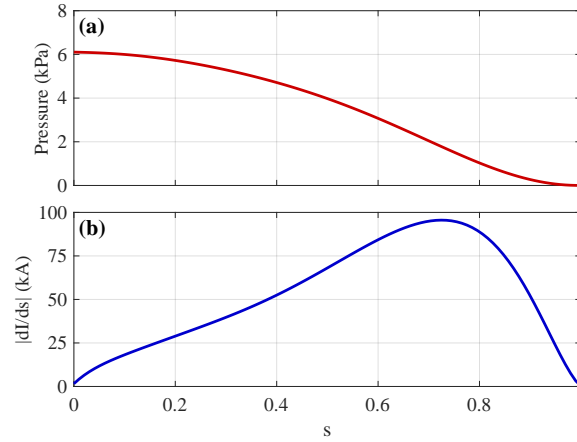


FIG. 9. Profiles of (a) plasma pressure and (b) the radial derivative of toroidal plasma current as a function of normalized toroidal flux  $s$  for the target plasma equilibrium.

solution and exhibit characteristics much closer to those of the targeted plasma. In particular, both Subsets 5 and 8 attain rotational transform profiles that remain within 0.03 of the target values, and their effective ripple, indicated by the metric  $\epsilon_{\text{eff}}^{3/2}$ , remains close to  $10^{-4}$  at the core and  $10^{-3}$  at the edge.

As indicated by the free-boundary equilibrium calculations in Fig. 8, Subset 8 does not yield a major improvement in field accuracy over Subset 5 despite having lower values of  $\|\theta_{\text{offs}}\|_2$ . On the other hand, Subset 5 would be substantially simpler to fabricate by virtue of consisting of half as many unique polarization types. For this reason, we adopted Subset 5 for further design, fabrication, and construction activities.

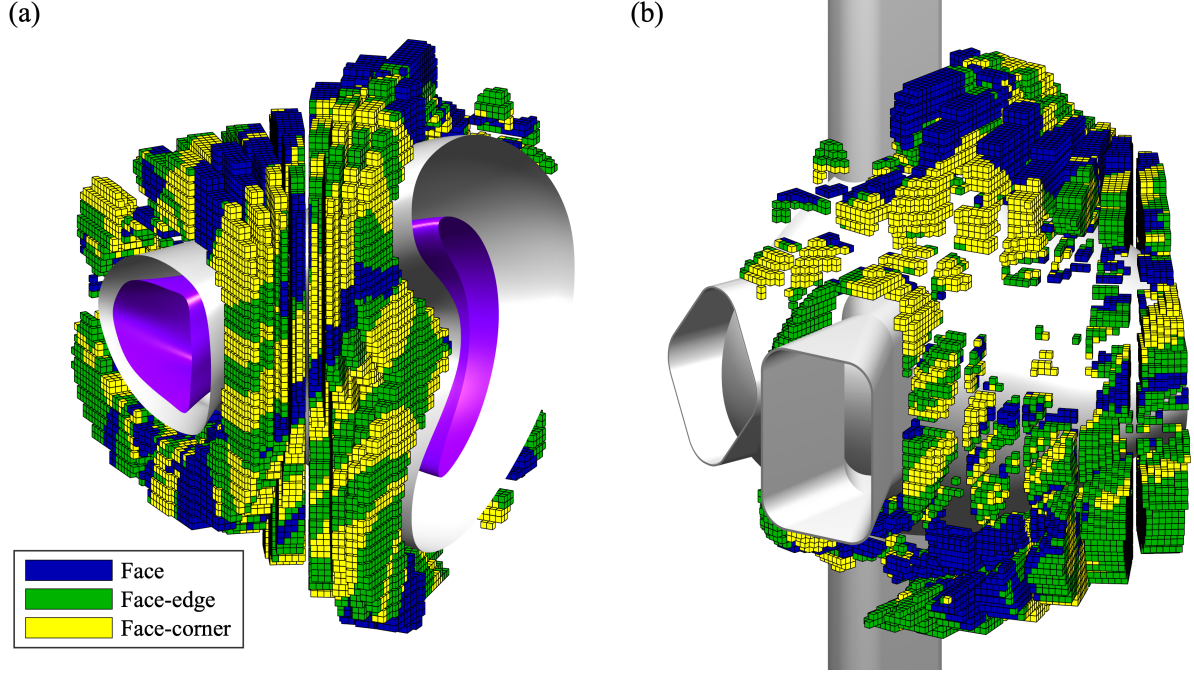


FIG. 10. Renderings of a discretized magnet solution for the target plasma, viewed from (a) the inboard side and (b) the outboard side. The cubic magnets are color-coded according to polarization type. Magnets with optimized dipole moments of magnitude zero, most of which were on the outboard side, have been omitted from the initial arrangement. The boundary of the plasma is also shown in purple.

The discretized solution using Subset 5—consisting of the face, face-edge, and face-corner polarization types—is shown in Fig. 10. The geometric layout of the magnets corresponds to the initial arrangement shown in Fig. 1, omitting the magnets that were given dipole moments of zero during the optimization procedure. Overall, the solution for one half-period contains 35,436 cubic magnets. These include 8,778 of the face polarization type (24.8%), 13,735 of the face-edge type (38.8%), and 12,923 of the face-corner type (36.5%). Extending this solution around the full stellarator (six half-periods), therefore, would require 212,616 magnets, constituting a magnet volume of  $5.74 \text{ m}^3$ .

An important practical consideration for stellarator design is whether the magnets can produce closed flux surfaces in the absence of plasma or plasma current. Vacuum flux surfaces greatly ease the requirements for plasma startup and operation at low beta, which are necessary conditions for reaching the target plasma equilibrium. Fortunately, the vacuum field from Subset 5 and the NCSX TF coils does indeed contain flux surfaces. This can be seen in Fig. 11, which shows Poincaré cross-sections of magnetic field lines at two toroidal positions. The FIELDLINES code [30] was employed to compute the field line trajectories.

## VI. CONCLUSIONS AND FUTURE WORK

In this work, we have produced a design for an array of cubic magnets of three distinct types that confines a quasi-axisymmetric stellarator plasma. Our approach divided the task into three principal steps: (1) specification of the allowable positions, shapes, and geometric orientations of the magnets; (2) continuous optimization of the magnets' dipole moments; and (3) adjustment of the optimized dipole moments to conform to certain allowable polarization types. Several subsets of polarization types were considered, and ultimately a subset consisting of three distinct types was chosen that exhibited high field accuracy while limiting the complexity of fabrication.

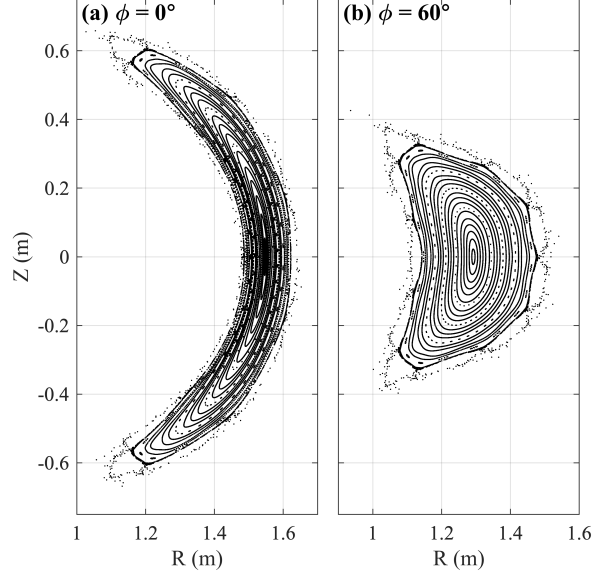


FIG. 11. Cross-sections of magnetic field lines traced in the vacuum field produced by the magnets from the discretized solution with polarizations from Subset 5 and the NCSX TF coils at toroidal angles (a)  $\phi = 0^\circ$  and (b)  $\phi = 60^\circ$ .

The design of a magnet array for a variant of an NCSX plasma equilibrium was the primary motivating factor for the work described in this paper. However, the procedures developed here are broadly generalizable to any stellarator plasma configuration, as long as the magnitudes of the required shaping fields are within the capabilities of existing permanent magnet materials. Whether or not rare-Earth magnets are capable of confining a given target plasma depends on its magnetic and structural requirements. The magnetic requirements include the on-axis toroidal field strength, the amount of external poloidal field shaping required for a given on-axis field strength, and whether or not toroidal-field coils contribute to the external poloidal field (as is the case with, for example, the tilted coils used in the concept proposed in Ref. [14]). Key structural considerations include the amount of spacing required between the plasma vessel and the magnet array and the amount of spacing required between the magnets themselves for structural supports.

The optimization procedure developed in this work achieves a similar end goal to that developed by Lu et al. [21] for designing stellarators with cubic magnets with discrete polarizations. A common aspect of both approaches is that they entail optimizing the dipole moments of an arrangement of magnets with prescribed locations and spatial orientations. However, the optimization procedures differ. In Ref. [21], the dipole moments are optimized in two stages: first, the dipole moment of each magnet is iteratively adjusted to minimize the normal field at a nearby location on the plasma boundary; and second, the iterative adjustments on each magnet are repeated to minimize the global residual quantity  $\chi_B^2$  (as defined in Eq. 1). The iterative adjustments for each magnet involve cycling through the allowable discrete polarization vectors and choosing the one that yields the best result; hence, the approach is a fully discrete optimization procedure. By contrast, the approach described in this paper entails initial steps that utilize continuous optimization procedures (Sec. IV) to yield a solution with a continuous distribution of dipole moment directions, which are then adjusted to the nearest of a set of discrete vectors defined for each magnet (Sec. V). In addition, the procedure developed here only considers the global residual field error quantity  $\chi_B^2$  and does not include a stage that optimizes each magnet according to its local contribution to the field at the plasma boundary.

In this design study, the dipole moment optimizations and calculations of field accuracy treated each magnet as an ideal magnetic dipole, contributing in a fixed and linear way to the overall magnetic field distribution. In practice, the actual field generated by the magnet set will differ from the idealized calculations,

both as a result of the permeability of the magnets and, to some extent, slight demagnetization of some of the magnets in response to the external magnetic field. Furthermore, if such an array is to be fabricated and constructed, additional field errors will arise from imperfections in fabrication and spatial misalignments of the magnets within the mounting structure.

To correct for misalignments and nonlinear field effects, a secondary array of error-correction magnets is foreseen to be placed between the main magnet array and the plasma vessel. The main magnet array described in this paper was constrained to allow room for this additional set of magnets. This error-correcting array will be specified following the construction and assembly of the main magnet array, at which point the deviations of the field of the as-built array from the ideal prediction can be measured. The required dipole moments for these magnets can then be determined using the same procedure outlined in this paper for the main magnets. As will be described in detail in forthcoming publications, assessments of the sensitivity of the magnetic field to positional offsets [31], simulations of possible positional magnet offsets [32], and finite-element models of the magnet array that account for finite magnet size, permeability, and demagnetization [26] have indicated that all of these deviations should be within the correction capabilities of the secondary array.

### ACKNOWLEDGMENTS

This work was supported by the Advanced Research Projects Agency – Energy (ARPA-E), U.S. Department of Energy, under contract number DE-AC02-09CH11466. The views and opinions of authors expressed herein do not necessarily state or reflect those of the U.S. Government or any agency thereof. The U.S. Government retains a non-exclusive, paid-up, irrevocable, world-wide license to publish or reproduce the published form of this manuscript, or allow others to do so, for U.S. Government purposes.

### CONFLICT OF INTEREST

A patent application (US 63/319,568) incorporating parts of this work has been filed by Princeton University and authors K.C.H., C.Z., and D.A.G.

### DATA AND CODE AVAILABILITY

The data presented in this paper are available at <http://arks.princeton.edu/ark:/88435/dsp01x059cb547>. The VMEC, NEO, and FIELDLINES codes are part of the STELLOPT suite of codes [33] and may be accessed at <https://github.com/PrincetonUniversity/STELLOPT>. Access to the MAGPIE and FAMUS codes may be given upon request.

- 
- [1] G. H. Nielson, C. O. Gruber, J. H. Harris, D. J. Rej, R. T. Simmons, and R. L. Strykowski, Lessons learned in risk management on NCSX, *IEEE Transactions on Plasma Science* **38**, 320 (2010).
  - [2] T. Rummel, K. Riße, G. Ehrke, K. Rummel, A. John, T. Mönnich, K.-P. Buscher, W. H. Fietz, R. Heller, O. Neubauer, and A. Panin, The superconducting magnet system of the stellarator Wendelstein 7-X, *IEEE Transactions on Plasma Science* **40**, 769 (2012).
  - [3] H.-S. Bosch, R. C. Wolf, T. Andreeva, J. Baldzuhn, D. Birus, T. Bluhm, T. Bräuer, H. Braune, V. Bykov, A. Cardella, F. Durodié, M. Endler, V. Erckmann, G. Gantenbein, D. Hartmann, D. Hathiramani, P. Heimann, B. Heinemann, C. Hennig, M. Hirsch, D. Holtum, J. Jagielski, J. Jelonnek, W. Kasperek, T. Klinger, R. König, P. Kornejew, H. Kroiss, J. G. Krom, G. Kühner, H. Laqua, H. P. Laqua, C. Lechte, M. Lewerentz, J. Maier, P. McNeely, A. Messina, G. Michel, J. Ongena, A. Peacock, T. S. Pedersen, R. Riedl, H. Riemann, P. Rong,

- N. Rust, J. Schacht, F. Schauer, R. Schroeder, B. Schweer, A. Spring, A. Stäbler, M. Thumm, Y. Turkin, L. Wegener, A. Werner, D. Zhang, M. Zilker, and et al., Technical challenges in the construction of the steady-state stellarator Wendelstein 7-X, *Nuclear Fusion* **53**, 126001 (2013).
- [4] N. Pomphrey, L. Berry, A. Boozer, A. Brooks, R. E. Hatcher, S. P. Hirshman, L.-P. Ku, W. H. Miner, H. E. Mynick, W. Reiersen, D. J. Strickler, and P. M. Valanju, Innovations in compact stellarator coil design, *Nuclear Fusion* **41**, 339 (2001).
  - [5] T. Brown, J. Breslau, D. Gates, N. Pomphrey, and A. Zolfaghari, Engineering optimization of stellarator coils lead to improvements in device maintenance, in *26th IEEE Symposium on Fusion Engineering (SOFE)* (2015).
  - [6] D. A. Gates, A. H. Boozer, T. Brown, J. Breslau, D. Curreli, M. Landreman, S. A. Lazerson, J. Lore, H. Mynick, G. H. Neilson, N. Pomphrey, P. Xanthopoulos, and A. Zolfaghari, Recent advances in stellarator optimization, *Nuclear Fusion* **57**, 126064 (2017).
  - [7] C. Zhu, S. R. Hudson, Y. Song, and Y. Wan, New method to design stellarator coils without the winding surface, *Nuclear Fusion* **58**, 016008 (2018).
  - [8] M. Landreman, An improved current potential method for fast computation of stellarator coil shapes, *Nuclear Fusion* **57**, 046003 (2017).
  - [9] E. J. Paul, M. Landreman, A. Bader, and W. Dorland, An adjoint method for gradient-based optimization of stellarator coil shapes, *Nuclear Fusion* **58**, 076015 (2018).
  - [10] J.-F. Lobsien, M. Drevlak, T. S. Pedersen, and the W7-X team, Stellarator coil optimization towards higher engineering tolerances, *Nuclear Fusion* **58**, 106013 (2018).
  - [11] T. G. Kruger, C. Zhu, A. Bader, D. T. Anderson, and L. Singh, Constrained stellarator coil curvature optimization with FOCUS, *Journal of Plasma Physics* **87**, 175870201 (2021).
  - [12] N. Lonigro and C. Zhu, Stellarator coil design using cubic splines for improved access to the outboard side, *Nuclear Fusion* **62**, 066009 (2022).
  - [13] A. Giuliani, F. Wechsung, A. Cerfon, G. Stadler, and M. Landreman, Single-stage gradient-based stellarator coil design: optimization for near-axis quasisymmetry, *Journal of Computational Physics* **459**, 111147 (2022).
  - [14] P. Helander, M. Drevlak, M. Zarnstorff, and S. C. Cowley, Stellarators with permanent magnets, *Physical Review Letters* **124**, 095001 (2020).
  - [15] C. Zhu, M. Zarnstorff, D. Gates, and A. Brooks, Designing stellarators using perpendicular permanent magnets, *Nuclear Fusion* **60**, 076016 (2020).
  - [16] M. Landreman and C. Zhu, Calculation of permanent magnet arrangements for stellarators: a linear least-squares method, *Plasma Physics and Controlled Fusion* **63**, 035001 (2021).
  - [17] G. S. Xu, Z. Y. Lu, D. H. Chen, L. Chen, X. Y. Zhang, X. Q. Wu, M. Y. Ye, and B. N. Wan, Design of quasi-axisymmetric stellarators with varying-thickness permanent magnets based on Fourier and surface magnetic charges method, *Nuclear Fusion* **61**, 026025 (2021).
  - [18] P. Merkel, Solution of stellarator boundary value problems with external currents, *Nuclear Fusion* **27**, 867 (1987).
  - [19] C. Zhu, K. C. Hammond, M. Zarnstorff, T. Brown, D. Gates, K. Corrigan, M. Sibilia, and E. Feibush, Topology optimization of permanent magnets for stellarators, *Nuclear Fusion* **60**, 106002 (2020).
  - [20] Z. Y. Lu, G. S. Xu, D. H. Chen, L. Chen, X. Y. Zhang, M. Y. Ye, and B. N. Wan, Design of quasi-axisymmetric stellarators with variable-thickness perpendicular permanent magnets based on a two-step magnet design strategy, *Nuclear Fusion* **61**, 106028 (2021).
  - [21] Z. Y. Lu, G. S. Xu, D. H. Chen, X. Y. Zhang, L. Chen, M. Y. Ye, H. Y. Guo, and B. N. Wan, Development of advanced stellarator with identical permanent magnet blocks, *Cell Reports Physical Science* **3**, 100709 (2022).
  - [22] T. Qian, M. Zarnstorff, D. Bishop, A. Chambliss, A. Dominguez, C. Pagano, D. Patch, and C. Zhu, Simpler optimized stellarators using permanent magnets, *Nuclear Fusion* **62**, 084001 (2022).
  - [23] K. C. Hammond, C. Zhu, T. Brown, K. Corrigan, D. A. Gates, and M. Sibilia, Geometric concepts for stellarator permanent magnet arrays, *Nuclear Fusion* **60**, 106010 (2020).
  - [24] M. C. Zarnstorff, L. A. Berry, A. Brooks, E. Fredrickson, G.-Y. Fu, S. Hirshman, S. Hudson, L.-P. Ku, E. Lazarus, D. Mikkelsen, D. Monticello, G. H. Neilson, N. Pomphrey, A. Reiman, D. Spong, D. Strickler, A. Boozer, W. A. Cooper, R. Goldston, R. Hatcher, M. Isaev, C. Kessel, J. Lewandowski, J. F. Lyon, P. Merkel, H. Mynick, B. E. Nelson, C. Nührenberg, M. Redi, W. Reiersen, P. Rutherford, R. Sanchez, J. Schmidt, and R. B. White, Physics of the compact advanced stellarator NCSX, *Plasma Physics and Controlled Fusion* **43**, A237 (2001).
  - [25] B. E. Nelson, L. A. Berry, A. B. Brooks, M. J. Cole, J. C. Chrzanowski, H.-M. Fan, P. J. Fogarty, P. L. Goranson, P. J. Heitzenroeder, S. P. Hirshman, G. H. Jones, J. F. Lyon, G. H. Nielson, W. T. Reiersen, D. J. Strickler,



- and D. E. Williamson, Design of the national compact stellarator experiment (NCSX), *Fusion Engineering and Design* **66-68**, 169 (2003).
- [26] C. Zhu, K. C. Hammond, A. Rutkowski, K. Corrigan, D. Bishop, A. Brooks, P. Dugan, R. Ellis, L. Perkins, Y. Zhai, A. Chambliss, D. A. Gates, D. Steward, C. Miller, B. Lown, and R. Mercurio, PM4STELL: a prototype permanent magnet stellarator structure, *Physics of Plasmas* **29**, 112501 (2022).
  - [27] S. P. Hirshman and J. C. Whitson, Steepest-descent moment method for three-dimensional magnetohydrodynamic equilibria, *Physics of Fluids* **26**, 3553 (1983).
  - [28] S. P. Hirshman, W. I. van Rij, and P. Merkel, Three-dimensional free boundary calculations using a spectral Green's function method, *Computer Physics Communications* **43**, 143 (1986).
  - [29] V. V. Nemov, S. V. Kasilov, W. Kernbichler, and M. F. Heyn, Evaluation of  $1/\nu$  neoclassical transport in stellarators, *Physics of Plasmas* **6**, 4622 (1999).
  - [30] S. A. Lazerson, M. Otte, S. Bozhnikov, C. Biedermann, T. S. Pedersen, and the W7-X team, First measurements of error fields on W7-X using flux surface mapping, *Nuclear Fusion* **56**, 106005 (2016).
  - [31] A. Chambliss, C. Zhu, D. Gates, M. Zarnstorff, and T. Qian, Sensitivity of magnetic islands in permanent magnet stellarators using the gradient and Hessian methods, under review.
  - [32] A. Rutkowski, K. Hammond, C. Zhu, D. A. Gates, and A. Chambliss, A novel scheme for error field correction in permanent magnet stellarators, under review.
  - [33] S. A. Lazerson, J. Schmitt, C. Zhu, J. Breslau, and STELLOPT Developers, STELLOPT, <https://doi.org/10.11578/dc.20180627.6> (2020).